



Sea Surface Heights and Marine Gravity Determined from SARAL/AltiKa Ka-band Altimeter Over South China Sea

CHENGCHENG ZHU,¹ XIN LIU,¹ JINYUN GUO,¹ SHENGWEN YU,¹ YUPENG NIU,¹ JIAJIA YUAN,¹ ZHEN LI,¹ and YONGGANG GAO²

Abstract—SARAL/AltiKA (SRL) is the first altimetry satellite with a Ka-band altimeter. To validate the advantages of the Ka-band altimeter over traditional Ku-band altimeters in marine geodetic applications, a comprehensive analysis is carried out over the South China Sea (SCS) (0–30° N, 105–125° E) from three aspects, namely the influence of load on waveforms, the precision of sea surface heights (SSHs), and the precision of altimeter-derived marine gravity field. Coastal waveforms of SRL, Jason-2, and CryoSat-2 are separately compared with corresponding ocean-type waveforms. The radius of coastal influence on SSHs of SRL/exact repeat mission (SRL/ERM) is the smallest, being about 3 km. Crossover discrepancies, global mean sea surface models, and tide gauge data are used to assess the precision of altimetric SSHs. Compared with the SSH precision of Ku-band Jason-2/ERM, the SSH precision of Ka-band SRL/ERM is 4.6% higher over the SCS and 10% higher in offshore areas. Gridded gravity anomalies are derived from measurements of SRL/drifted phase (SRL/DP) and CryoSat-2 through the inverse Vening-Meinesz formula, respectively. According to the assessment by shipborne gravity data and global marine gravity models, the precision of SRL/DP-derived gravity is higher than that of CryoSat-2-derived gravity over the SCS, especially in offshore areas. In some cycles, ground tracks of SRL/ERM have large drifting of more than 10 km from nominal tracks. The results show that the Ka-band altimeter of SRL has better precision in SSHs and marine gravity recovery than the Ku-band altimeter over the SCS, particularly in offshore areas.

Keywords: SARAL/AltiKA, Ka-band altimeter, Sea surface height, Marine gravity, Waveform, South China Sea.

1. Introduction

Sea surface heights (SSHs) can be retrieved from satellite altimetry technology with increasing precision and accuracy. Since the 1970s, about 20 altimetry satellites have been launched, and a significant amount of altimeter data obtained. The mean sea surface and its variations can be researched directly on the basis of altimetric SSHs (Schaeffer et al. 2012; Andersen and Knudsen 2015; Guo et al. 2015; Andersen et al. 2018; Lickley et al. 2018; Pujol et al. 2018; Yuan et al. 2020), which is fundamental for studying mean dynamic topography (Hernandez & Schaeffer, 2001; Guo et al. 2010; Kosempa and Chambers 2014). Sea surface slopes can be calculated by differentiation between along-track adjacent SSHs to reduce long-wavelength errors of SSHs. Along-track slopes are used to determine deflections of the vertical (DOVs), which are directly used to derive marine gravity (Hwang, 1998; Hwang and Chang 2014; Sandwell et al. 2019; Zhu et al. 2019).

SARAL/AltiKA (SRL), the first altimetry satellite operating in the Ka band (35.75 GHz), was launched in February 2013. The AltiKa altimeter carried on SRL is the successor of the Sival altimeter of CryoSat and the Poseidon3 altimeter of Jason-2 (CNES, 2016). Compared with traditional Ku/C altimeters, the Ka altimeter with higher frequency has a smaller altimeter footprint, leading to better spatial resolution. The AltiKa altimeter's enhanced bandwidth of 500 MHz results in higher vertical resolution and higher pulse repetition frequency. Absolute calibrations (Babu, 2014), SSH assessments (Prandi et al. 2015), and retracking methods (Zhang and Sandwell

Supplementary Information The online version contains supplementary material available at <https://doi.org/10.1007/s00024-021-02709-y>.

¹ College of Geodesy and Geomatics, Shandong University of Science and Technology, Qingdao 266590, People's Republic of China. E-mail: xinliu1969@126.com; jinyunguo1@126.com

² College of Environment and Resources, Fuzhou University, Fuzhou 350116, People's Republic of China.

2016), and geoid derivation (Smith, 2015) have been studied separately. However, there are few systematic studies on the effect of coastlines on SRL-measured waveforms, the precision of SRL-measured SSH, and the performance of SRL in deriving marine gravity.

The complicated submarine topography and abundant islands in the South China Sea (SCS) affect the precision of altimetry data and altimeter-derived marine gravity (Morton and Blackmore 2001; Hsiao et al. 2016). Therefore, the SCS and its adjacent ocean, covering 105–125° E and 0–30° N, are selected as the research area to compare Ka-band altimeters with Ku altimeters. Section 2 introduces the data used in this study. In Sect. 3, methods for preprocessing and deriving gravity are presented in detail. In Sect. 4, coastal waveforms of SRL, Jason-2, and CryoSat-2 are used to study the radius of coastal influence on altimeter data. In Sect. 5, crossover discrepancies, mean sea surface (MSS) models, and in situ tide gauge records are used to evaluate the precision of SSHs of exact repeat mission (ERM) from Jason-2 and SRL. In Sect. 6, marine gravity models on a 1' × 1' grid are derived from geodetic mission (GM) SSHs of SRL and CryoSat-2, respectively. Finally, the shipborne gravity and recognized global marine gravity models are used to assess the precision of altimeter-derived marine gravity.

2. Study Data

2.1. Altimeter Data

ERM data have characteristics of high observation precision and exact repeated tracks, so ERM-measured SSHs are used to assess the performance of Ka-band and Ku-band altimeters in SSH observations. As TOPEX/JASON series altimetry satellites (including Topex/Poseidon, Jason-1, Jason-2, and Jason-3) offer continuous observations and high observation precision, 20-year (1993–2012) long-wavelength MSS is determined from TOPEX/JASON mean profiles within the 65° parallels (Andersen, Jain, et al., 2015). Therefore, Jason-2/ERM altimeter data are compared with SRL/ERM data over the same period.

As GM-measured data have high spatial resolution, the SRL altimeter data in drifting phase (DP) are

used to study the precision of SRL-derived marine gravity. CryoSat-2 provides a nominal track interval of about 2.5 km and plays a major role in global altimetric marine gravity model construction (Sandwell et al. 2014). Therefore, the marine gravity derived from CryoSat-2 data on low-resolution mode (LRM) is compared with that derived from SRL/DP data over the same period. Information about SRL/ERM, Jason-2/ERM, SRL/DP, and CryoSat-2/LRM is listed in Table 1.

Waveforms of Jason-2 and SRL can be obtained from archiving validation and interpretation of satellite oceanographic data (AVISO) (<ftp://ftp-access.aviso.altimetry.fr>). Meanwhile, waveforms of CryoSat-2 are released by European Space Agency (<ftp://science-pds.cryosat.esa.int>). Tracking gates, sampling frequency, and other information about waveforms are listed in Table 1.

SSHs of Level2 plus (L2P) products (CNES 2017) at 1-Hz sampling frequency, available at AVISO, are used in this study to evaluate advantages of SRL altimeter. L2P products of Jason-2/ERM and SRL/ERM listed in Table 2 are used to evaluate the precision of SSHs, whose ground tracks are shown in Fig. 1. Meanwhile, L2P products of SRL/DP and CryoSat-2 listed in Table 2 are used to study altimeter-derived marine gravity. Due to dense ground tracks of GMs, Fig. 2 only shows tracks of SRL/DP and CryoSat-2 in the region covering 12–14° N and 112–114° E.

Table 1
Information about altimetry satellites

Contrastive parameters	SRL/ERM and DP	Jason-2/ERM	Cryosat-2/LRM
Altimeter	AltiKa	Poseidon3	Siral
Frequency (GHz)	35.75	13.575/5.3	13.575
Altitude (km)	800	1336	717
Inclination (°)	98.55	66	92
Pulse repetition frequency (Hz)	3600	2100	1970
Bandwidth (MHz)	500	320	320
Antenna footprint diameter (km)	9	21	15
Pulse footprint diameter (km)	1.4	2.2	1.7
Gate number	128	104	128
Sampling frequency (Hz)	40	20	20

Table 2
Specifications of L2p products of altimetry satellites

Contrastive parameters	SRL/ERM	Jason-2/ERM	SRL/DP	Cryosat-2
Cycles	1–35	173–294	80–107	100–121
Period	14 March 2013 to 4 July 2016	13 March 2013 to 5 July 2016	4 July 2016 to 10 July 2018	4 July 2016 to 10 July 2018
Observation number	555,539	574,878	321,881	358,901
Orbit	GDR-E			
Dry tropospheric correction	ECMWF			
Wet tropospheric correction	Neural network correction	Neural network correction	Neural network correction	ECMWF
Ionosphere correction	GIM	Dual-frequency	GIM	GIM
Tide correction	Ocean tide: FES2014 solid Earth tide: Cartwright and Edden (1973) pole tide: Desai et al. (2015)			
Ocean environmental correction	Sea state bias (SSB): nonparametric Inverse barometer correction: ECMWF High-frequency fluctuations: Mog2D model			

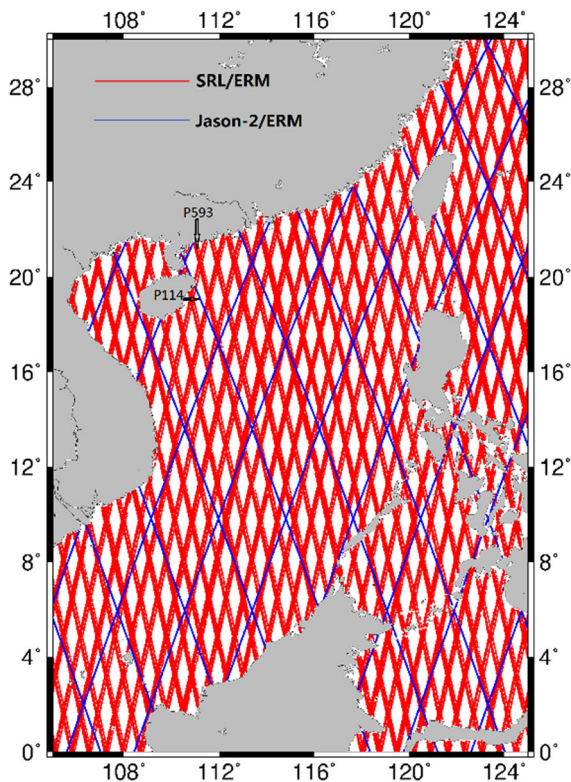


Figure 1
Ground tracks of SRL/ERM and Jason-2/ERM around the SCS

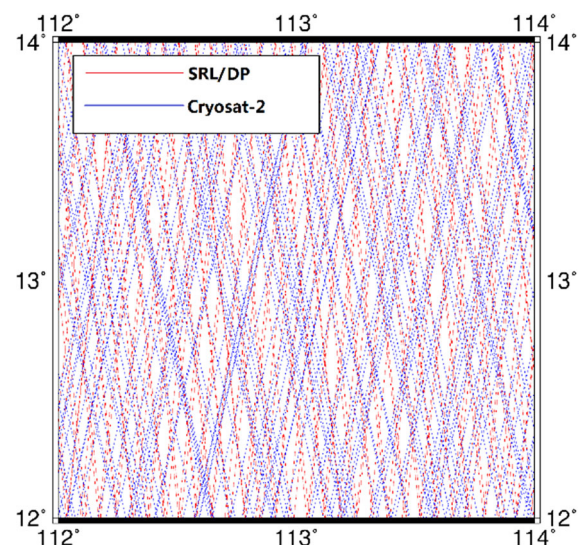


Figure 2
Ground tracks of SRL/DP and CryoSat-2

2.2. Other Data

2.2.1 MSS Model

MSS models can be used to assess the precision of SSH observations. We use the newly released model of DTU18MSS (Andersen et al. 2018) published by Technical University of Denmark (DTU). DTU18MSS is referenced to the period 1993–2012 (Pujol et al. 2018). Signals of the MSS model at long

wavelengths are from ERM data, while those at short wavelengths are from GM data.

2.2.2 Tide Gauge Records

Tide gauge (TG) records are independent of altimeter data and can be consequently used to assess the precision of SSHs. TG data are released by University of Hawaii Sea Level Center (<https://uhslc.soest.hawaii.edu/>). As the research quality data are considered to be the final science-ready datasets (Caldwell et al. 2015), they are used for TG–altimetry comparison.

2.2.3 Gravity Data

The Earth gravitational field model 2008 (EGM2008) (Pavlis et al. 2012) is selected as the reference gravity field, following previous studies (Sandwell et al. 2013; Shih et al. 2015). Moreover, the shipborne gravity and global marine gravity models are used to assess altimeter-derived gravity.

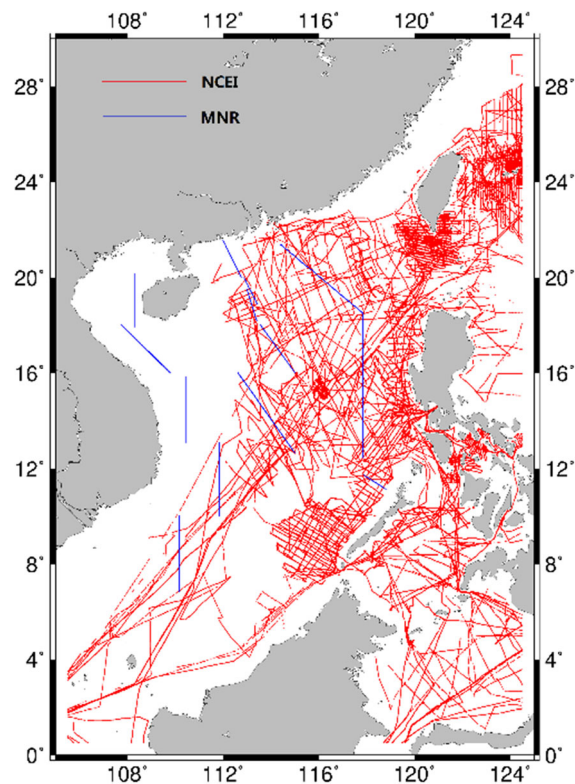


Figure 3
Tracks of shipborne gravity

The shipborne gravity data shown in Fig. 3 are provided by US National Centers for Environmental Information (NCEI) and Ministry of Natural Resources (MNR) of P. R. China. Shipborne gravity data have some long-wavelength errors that are caused by drifts in gravimeter readings, off-leveling, incorrect ties to base stations, and different reference fields. EGM2008 is adopted to unify the reference datum and correct long-wavelength errors for each cruise by using a quadratic polynomial regression (Hwang & Parsons, 1995).

Ma rine gravity model SIO V27.1 (Sandwell et al. 2014), released by Scripps Institution of Oceanography (SIO) in 2019, is selected as assessment data for altimeter-derived gravity. SIO V27.1 is on a $1' \times 1'$ grid with accuracy of 2 mGal in the global.

3. Study Method

3.1. Altimeter Data Preprocessing

L2P products released by AVISO have the same reference ellipsoid, so SSHs can be calculated from satellite altitude measurements and range measurements by only applying geophysical corrections and propagation corrections. Altimetric SSHs used to calculate crossover discrepancies, compare with MSS models, and derive gravity can be calculated by

$$H_0 = H_{\text{alt}} - (H_{\text{range}} + \Delta H_{\text{atm}} + \Delta H_{\text{SET}} + \Delta H_{\text{PT}} + \Delta H_{\text{LT}} + \Delta H_{\text{EOT}} + \Delta H_{\text{SBS}} + \Delta H_{\text{DA}}) \quad (1)$$

where H_{alt} is the altitude of altimetry satellite; H_{range} is the range from a satellite to sea surface at the substellar point, which includes all instrumental corrections; ΔH_{atm} is the propagation correction including dry tropospheric, wet tropospheric, and ionosphere corrections; ΔH_{SET} , ΔH_{PT} , and ΔH_{EOT} are solid Earth tide, pole tide, and ocean tide corrections, respectively; ΔH_{LT} is the ocean tide loading correction, ΔH_{SBS} is the sea state bias correction; and ΔH_{DA} is the dynamic atmosphere correction.

TG records are sea level values without the ocean tide and dynamic atmosphere corrections, so altimetric SSHs used to compare with TG data can be calculated by

$$H_1 = H_{\text{alt}} - (H_{\text{range}} + \Delta H_{\text{atm}} + \Delta H_{\text{SET}} + \Delta H_{\text{PT}} + \Delta H_{\text{LT}} + \Delta H_{\text{SBS}}) \quad (2)$$

3.2. Marine Gravity Derivation

The inverse Vening-Meinesz formula (IVM) (Hwang, 1998) is used to derive gravity from altimeter data. First, SSHs calculated using Eq. (1) are filtered by Gaussian filtering (Hwang et al., 2002) with a convolution window radius of 7 km (Zhu et al., 2020). Then, geoid heights can be calculated from filtered SSHs by removing the mean dynamic topography model MDT_CNES-CLS13 (Rio et al. 2014). The difference between geoid heights at two along-track adjacent points is divided by the corresponding spherical distance to obtain the geoid gradient.

Second, residual geoid gradients are calculated from geoid gradients by removing reference geoid gradients. Gridded residual DOVs can be obtained by

$$\begin{pmatrix} \xi_{\text{res}} \\ \eta_{\text{res}} \end{pmatrix} = \begin{pmatrix} C_{\xi e} \\ C_{\eta e} \end{pmatrix} (C_{ee} + C_n)^{-1} e_{\text{res}} \quad (3)$$

where e_{res} is the residual geoid gradient, C_n is the noise variance of geoid gradients, and C_{ee} is the covariance matrix of geoid gradients; ξ_{res} and η_{res} are residual meridian and prime vertical components of DOVs, respectively; $C_{\xi e}$ and $C_{\eta e}$ are covariance matrices for meridian components–geoid gradients and vertical components–geoid gradients, respectively.

Finally, the residual gravity anomaly at point p can be determined from residual DOVs by

$$\Delta g(p) = \frac{\gamma_0}{4\pi} \iint_{\sigma} H'(\psi) (\xi_q \cos \alpha_{qp} + \eta_q \sin \alpha_{qp}) d\sigma_q \quad (4)$$

where ξ_q and η_q are the residual meridian component and the prime vertical component of DOVs at point q , respectively. γ_0 is the normal gravity at p , and the azimuth from q to p is α_{qp} . The kernel function $H'(\psi)$ is the function of spherical distance ψ . The final gravity anomalies can be obtained from residual gravity by restoring the reference gravity. The method for deriving gravity is shown in Fig. 4.

4. Waveforms

Altimetric echoes of SRL, Jason-2, and CryoSat-2 have well-defined shapes in the open sea and can be modeled by the Brown model (Brown, 1977). A waveform shape in the open sea has a sharp rising leading edge and then a gradual decline in the ramping edge. When there are islands and other non-ocean sea surfaces in the footprint, the reflected energy is in non-Brown style, leading to low precision of range measurements.

The waveform data of SRL/ERM, Jason-2/ERM, SRL/DP, and CryoSat-2 are used to study the radius of coastal influence. The contrastive tracks are selected according to the following principles: First, both tracks are from land to sea or from sea to land. Second, the intersection of the two tracks are close to the coastline. Following these principles, four groups of waveform data are selected for comparison, as listed in Table 3. The tracks in case A and case C approach land from ocean, and those in case B and case D approach ocean from land. The ground tracks are shown in Fig. 5.

The normalized altimetric echo power of each group within 30 km from the coastline is shown in Fig. 6. The distribution of echo power in various gates as a function of distance from the coast can be obtained from Fig. 6. Compared with the ocean-type waveforms in Fig. 7, the starting positions of contaminated waveforms are shown by gray vertical lines in Fig. 6. When observations get closer to the coastline, waveforms are contaminated more seriously.

It is shown in Fig. 6 that the contaminated waveform of SRL begins to occur approximately 3 km from a coastline. The contamination on waveforms of Jason-2 and CryoSat-2 starts approximately 9 km and 6 km from the coastline, respectively. The distances are almost consistent with the antenna footprint radius (Table 1) of the corresponding satellite. It can be concluded that the influence radius of coastlines decreases when the antenna footprint radius decreases. Therefore, the radius of coastal influence for SRL is the smallest, which leads to high-precision SSH measurements in offshore areas.

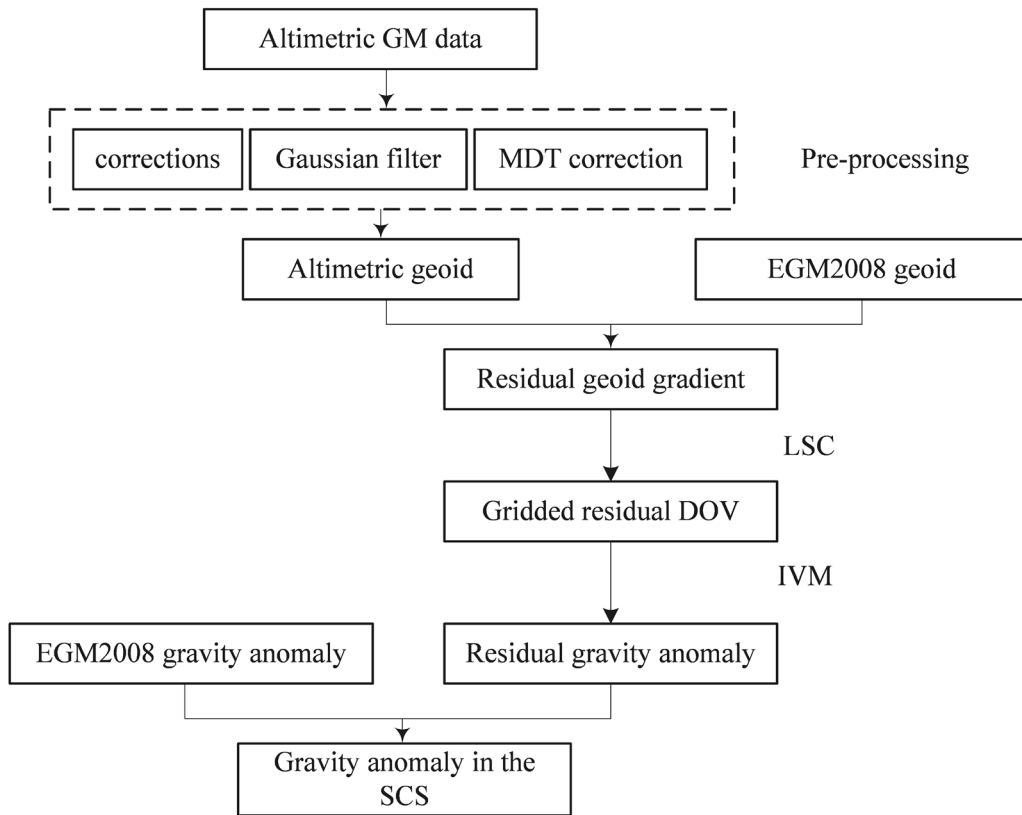


Figure 4
Method of gravity derivation from altimeter data

Table 3

Groups of waveform data

Groups	SRL/ERM	Jason-2/ERM	SRL/ DP	CryoSat-2
Case A	cycle2_pass221	cycle180_pass77		
Case B	cycle2_pass765	cycle180_pass51		
Case C			cycle102_pass383	cycle87_pass339
Case D			cycle102_pass355	cycle85_pass21

5. Altimetric SSHs

The precision of altimetric SSHs can be evaluated by crossover discrepancies, comparison with MSS models, and comparison with TG-measured SSHs.

5.1. Crossover Discrepancies

Analysis of crossover discrepancies is a common method to evaluate the precision of altimetric SSHs,

reflecting the consistency of SSH observations. Jason-2/ERM-measured and SRL/ERM-measured SSHs are calculated using Eq. (1) without collinear adjustments. Due to the temporal oceanic variability, crossover discrepancies are only calculated from SSHs of two tracks whose observation interval is less than 10 days. As listed in Table 4, the standard deviation (STD) of discrepancies for SRL/ERM is 3 mm smaller than that for Jason-2/ERM in the research area, which indicates that the precision of

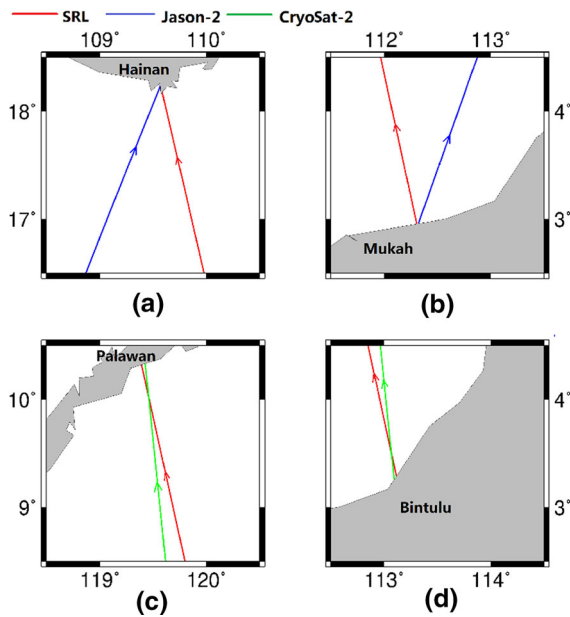


Figure 5

Ground tracks of waveform data. **a–d** represent ground tracks of case A, case B, case C, and case D, respectively

SRL/ERM-measured SSHs is approximately 3.7% higher than that of Jason-2/ERM-measured SSHs in the SCS. Considering the coastal influence on SSH precision, crossover discrepancies within 15 km from the coastline are listed in Table 4. The STD of discrepancies for SRL/ERM is 0.104 m, which is 10.3% smaller than that for Jason-2/ERM.

The results suggest that the SSH precision of SRL over the SCS is superior to that of Jason-2, which is consequent on its higher operating frequency. The SSH precision of SRL/ERM is significantly higher than that of Jason-2 /ERM in offshore areas, which can be attributed to two reasons: one is the smaller footprint of SRL that improves the spatial resolution and reduces the contamination of waveforms by coastlines, and the other is the weaker penetration of Ka-band signals. The return signal reflected from the ocean floor in shallow water for Ka-band altimeters is weaker than that for Ku-band altimeters, so the return signal of Ka-band altimeters has a smaller impact on SSH observations.

Therefore, it can be inferred that the Ka-band altimeter carried on SRL has higher SSH precision than the Ku-band altimeter carried on Jason-2, especially in offshore areas.

5.2. Comparison with MSS Models

DTU18MSS is used to assess SSH precision of Jason-2/ERM and SRL/ERM. The differences between altimetric SSHs and DTU18MSS are listed in Table 5. While DTU18MSS is referenced to the period 1993–2012, ERM-measured SSHs in this study are from 2013 to 2016. Therefore, the differences between DTU18MSS and altimetric SSHs contain system errors caused by temporal oceanic variability, which leads to the large mean value of about 7 cm listed in Table 5.

The STD of differences (difference STD) between SRL/ERM-measured SSHs and DTU18MSS is 7 mm (5.6%) smaller than that when replacing SRL by Jason-2. Compared with DTU18MSS, the difference STD for SRL/ERM is 23 mm (9.8%) smaller than that for Jason-2/ERM within 15 km from the coastline. Meanwhile, the root mean square (RMS) for SRL/ERM is smaller than that for Jason2/ERM, compared with DTU18MSS. Therefore, a conclusion similar to that in Sect. 5.1 can be drawn that the SSH precision of SRL is superior to that of Jason-2 in the SCS, especially in offshore areas.

After precision has been analyzed in the spatial domain, differences between altimetric SSHs and DTU18MSS are analyzed in the frequency domain by the power spectral density (PSD). As SRL began drifting away from the historical ERM tracks in March 2015, SRL/ERM-measured SSHs after March 2015 are not used in any MSS model (Pujol et al. 2018). As Jason-2/ERM-measured SSHs in 2015 and 2016 are also not used in DTU18MSS (Andersen et al. 2018), Pass593 of SRL/ERM and Pass114 of Jason-2/ERM are selected as the study passes because of fewer missing observations, as shown in Fig. 2. Meanwhile, considering the distance between the two passes, the area covering 111.0–114.5° E and 11.0–19.0° N is selected as the study area. The mean PSD of differences between altimetric SSHs and DTU18MSS for the study passes from March 2015 to July 2016 in the study area is calculated, as shown in Fig. 8. Compared with DTU18MSS, PSD of differences for Jason-2/ERM-measured SSHs is greater than that for SRL/ERM-measured SSHs for wavelengths smaller than ~ 25 km. As the altimeter noise dominates for wavelengths smaller than ~ 25 km

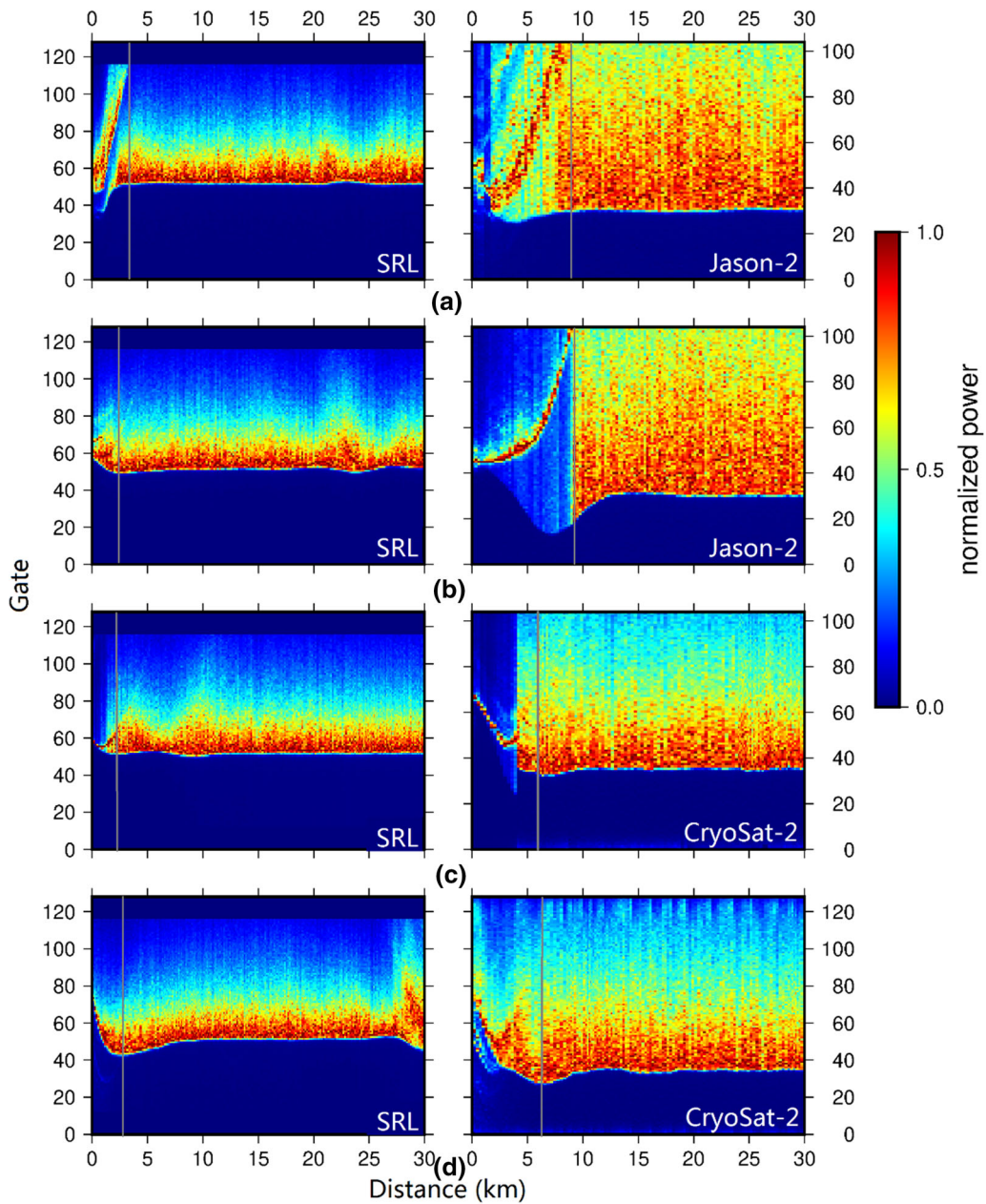


Figure 6

Waveform data of altimetry satellites. The abscissa is the distance from the coastline. **a–d** represent waveforms of case A, case B, case C, and case D, respectively

(Pujol et al. 2018), it can be concluded that the Ka-band altimeter carried on SRL has higher precision than the Ku-band altimeter carried on Jason-2.

5.3. Comparison with TG Records

The distance between TG station and satellite ground tracks should be taken into account for comparing altimetric SSHs with in situ TG records, and the waveform contamination by the complex

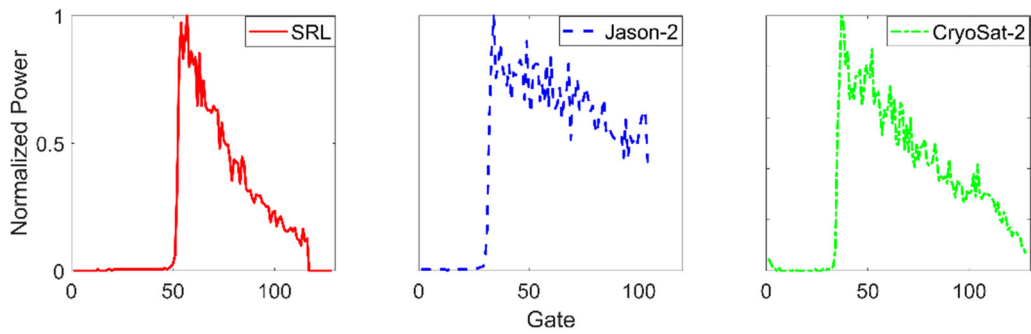


Figure 7
Ocean-type waveform of altimetry satellites

Table 4

Statistics of crossover differences under intramission situations

Distance from coastline (km)	Mission	Number	Mean (m)	STD (m)	RMS (m)
< 15	SRL/ERM	507	0.002	0.104	0.104
	Jason-2/ERM	573	0.000	0.116	0.116
≥ 0	SRL/ERM	5948	-0.002	0.078	0.078
	Jason-2/ERM	7434	0.000	0.081	0.081

coastline should be avoided. Therefore, the TG station of Ishigaki near an island is selected as the assessment TG station, as shown in Fig. 9. Moreover, the GNSS station of J750 is within 3 km of the TG station.

Figure 9 shows that ground tracks of Jason-2/ERM are well controlled, while tracks of SRL/ERM in some cycles have large drifting from nominal tracks. Although SRL/ERM is designed with the ground track control band of ±1 km (CNES, 2016), statistical analysis of the drifting in the SCS shows

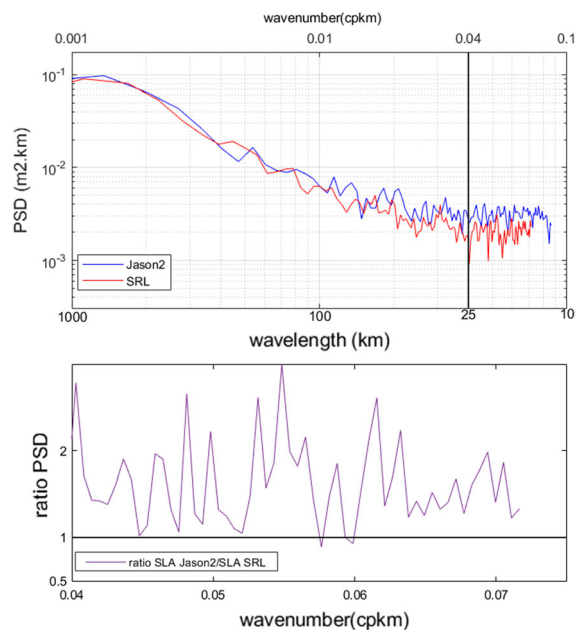


Figure 8
PSD and ratio PSD of differences between altimetric SSHs and DTU18MSS. The unit of wavenumber in the figure is cpkm, which represents km⁻¹

that the maximum ground track drifting of SRL/ERM is more than 10 km at the Equator. The maximum

Table 5

Statistics of differences between sea surface heights and DTU18

Distance from coastline (km)	Mission	Number	Mean (m)	STD (m)	RMS (m)
< 15	SRL/ERM	54,211	0.086	0.212	0.229
	Jason-2/ERM	59,401	0.079	0.235	0.248
≥ 0	SRL/ERM	555,539	0.070	0.118	0.138
	Jason-2/ERM	574,878	0.064	0.125	0.141

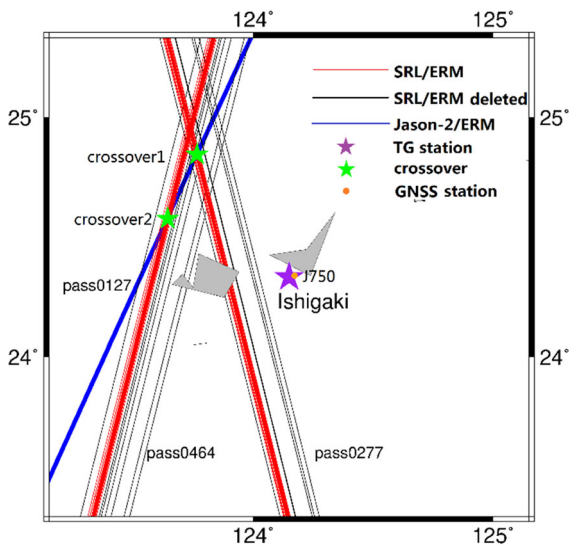


Figure 9
Ishigaki tide gauge and ground tracks of altimetry satellites

drifting is consistent with the drifting in the quality assessment report of cycle 024 (SARAL, 2015). Therefore, it is necessary to consider the drifting of ground tracks when processing ERM data of SRL.

As the distance between TG station and altimetric ground tracks affects the correlation between TG data and altimetric SSHs, SSHs at the crossovers of Jason-2/ERM and SRL/ERM tracks are used in this study. If a ground track drifts away too much from the nominal track, the SSH interpolated at the crossover will have a large error. Therefore, ground tracks with drifting greater than 5 km are deleted, as shown in Fig. 9 and listed in Table 6. Remaining ground tracks of SRL are shown in red in Fig. 9. Then, the crossover positions represented by green pentacles in Fig. 9 are determined from ground tracks of Jason-2 and remaining ground tracks of SRL. Along-track SSHs in different cycles are used to interpolate SSH at the crossover at the corresponding time, so the altimetric SSH time series at the crossover is

established. Meanwhile, TG records at the time corresponding to the altimetric time series are used to establish TG time series. If either of the altimetric data and TG data is missing at the same time, both of them at the corresponding time are rejected.

The datum planes of SSHs measured by TG stations and altimetry satellites are the revised local reference (zero reference level) and the surface of reference ellipsoid, respectively. Differences between geoid heights at different points are assumed to be constant, and differences between TG and altimetric datum planes are assumed to be constant. Therefore, it can be considered that the difference between altimetric SSH and TG data caused by different datum planes and positions is constant and can be eliminated by removing the mean value of time series. Residual time series shown in Fig. 10 are obtained by removing the corresponding mean value from original time series. The correlation coefficient and difference STD between altimeter residual series and corresponding TG residual series are calculated, and statistical results are listed in Table 7.

According to the difference STD and correlation coefficients listed in Table 7, the correlation between SRL/ERM series and TG series is stronger than that between Jason-2/ERM series and TG series. SRL/ERM has a cycle of about 35 days, while Jason-2/ERM has a cycle of about 10 days. To eliminate the effect of different cycle length on correlation, resampling Jason-2/ERM time series are obtained from Jason-2/ERM series by selecting data at a similar time of SRL/ERM time series. The correlation between resampling Jason-2/ERM and TG series is listed in Table 7, which is also slightly weaker than that between SRL/ERM series and TG series. Therefore, it can be inferred that SSH precision of SRL is slightly better than that of Jason-2.

Table 6

Information about crossovers

Crossover ID	Crossover coordinates	SRL/ERM		Jason-2/ERM	
		Pass	Cycle (drifting > 5 km)	Pass	Cycle (drifting > 5 km)
1	123.766° E, 24.844° N	Pass0277	24, 25, 30, 33, 34, 35	Pass0127	No
2	123.643° E, 24.577° N	Pass0464	17, 23, 24, 25, 30, 34, 35	Pass0127	No

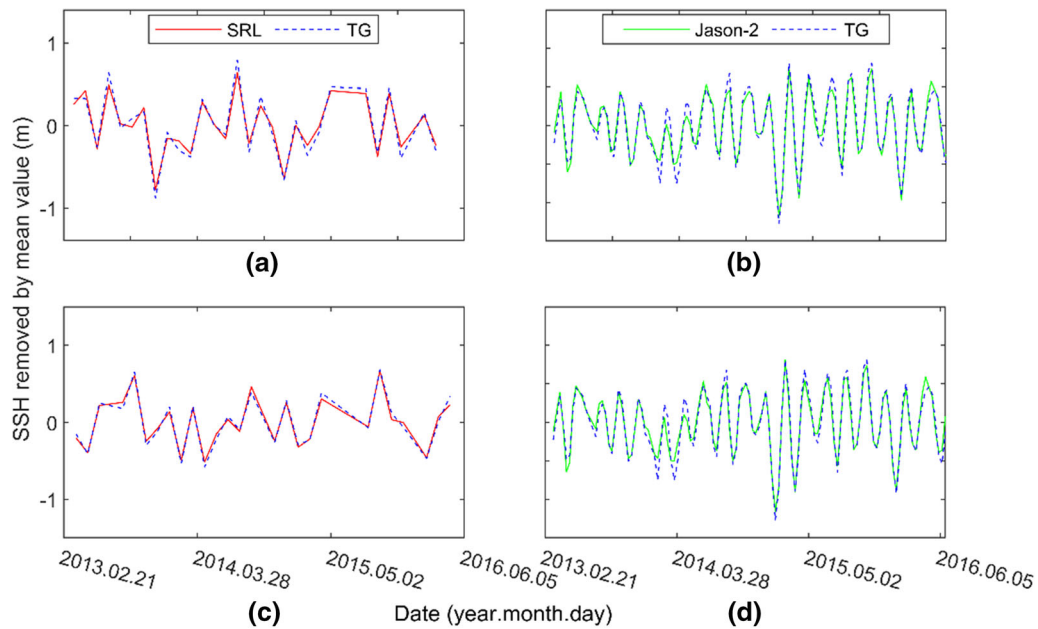


Figure 10

Time series of residual altimetric SSHs and TG data. **a, b** are the time series at Crossover1. **c, d** are the time series at Crossover2

Table 7

Statistics of correlation between TG and altimeter data

Crossover ID	Distance from TG (km)	Distance from coastline (km)	Satellite	STD (m)	Correlation coefficient
1	68.5	41.5	SRL	0.085	0.984
			Jason-2	0.095	0.975
			Jason-2 (resampling)	0.108	0.976
2	58.0	20.8	SRL	0.053	0.989
			Jason-2	0.093	0.977
			Jason-2 (resampling)	0.111	0.963

6. Precision of Altimeter-Derived Gravity

Gravity anomalies derived from SRL/DP data are compared with those derived from CryoSat-2 to validate the advantage of Ka-band altimeter carried on SRL in marine gravity derivation. First, geoid gradients are calculated from along-track SSHs of SRL/DP. Second, gridded DOVs are determined by the least-squares collocation method with calculation window size of 0.4° . Finally, DOVs are used to derive gravity on a $1' \times 1'$ grid by the IVM in the SCS. The gridded marine gravity anomalies from SSHs of SRL/DP are defined as GSRL, as shown in Fig. 11. The SSHs of CryoSat-2 during the same

period listed in Table 2 are also used to derive gridded marine gravity, which is defined as GC2.

Precision of GSRL and GC2 is assessed by shipborne gravity. The results are listed in Table 8. Evaluated by both NCEI and MNR shipborne gravity, the precision of GSRL is superior to that of GC2, which may be caused by the following reasons. First, as validated in Sect. 5, the SSH precision of Ka-band altimeter is better than that of Ku-band altimeter. Second, the direct data used in the marine gravity derivation are geoid gradients calculated from the difference between two adjacent along-track SSHs. The differentiation can weaken the influence of tropospheric correction errors, which can reduce the

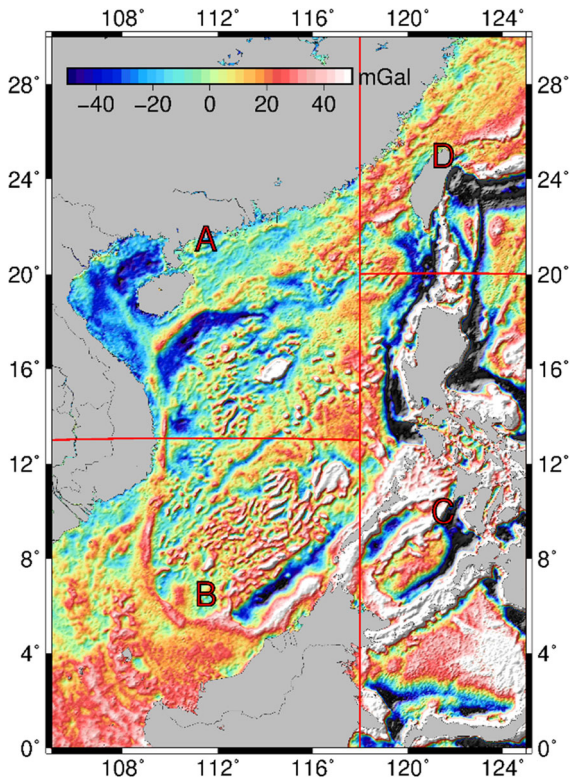


Figure 11
SRL/DP-derived gravity anomalies

Table 8

Differences between satellite-derived gravity and shipborne data (mGal)

Distance from coastline	Data	Max.	Min.	Mean	STD	RMS
≥ 0	GSRL-NCEI	41.98	-44.72	-0.07	5.59	5.59
	GC2-NCEI	43.16	-45.09	-0.11	5.71	5.71
	GSRL-MNR	15.70	-13.94	-0.05	2.58	2.59
	GC2-MNR	14.25	-14.72	-0.02	2.73	2.73
≤ 30 km	GSRL-NCEI	41.19	-42.31	-0.68	8.37	8.40
	GC2-NCEI	43.16	-45.09	-0.85	8.62	8.67

effects of sensitivity of Ka-band signal to rainy and cloudy conditions. Therefore, it can be concluded that

Table 9

Statistics of differences between satellite-derived and shipborne gravity in different regions (mGal)

Region	Data	Max.	Min.	Mean	STD	RMS
A	GSRL-NCEI	25.52	-35.28	0.08	4.67	4.67
	GC2-NCEI	23.01	-35.62	0.07	4.69	4.70
B	GSRL-NCEI	27.45	-34.36	-0.15	4.45	4.45
	GC2-NCEI	26.70	-34.23	-0.17	4.56	4.57
C	GSRL-NCEI	41.98	-44.72	-0.12	6.78	6.78
	GC2-NCEI	43.16	-45.09	-0.20	6.96	6.96
D	GSRL-NCEI	34.74	-39.24	-0.04	5.07	5.07
	GC2-NCEI	33.54	-36.21	-0.03	5.12	5.12

the precision of Ka-band altimeter-derived gravity is better than that of Ku-band altimeter-derived gravity.

The differences between altimetric and shipborne gravity within 30 km from coastline are also listed in Table 8 to study the influence of coastline on altimetric gravity. As MNR gravity data only have two cruises and 208 observation points in the area within 30 km from the coastline, coastal altimetric gravity anomalies are only assessed by NCEI data. Assessed by NCEI gravity, the precision of GSRL is 0.25 mGal higher than that of GC2 within 30 km from the coastline, and 0.12 mGal higher in the SCS. The results indicate that the precision of Ka-band altimeter-derived gravity is higher than that of Ku-band altimeter-derived gravity, particularly in off-shore areas.

As the complicated submarine topography and abundant islands in the SCS affect the precision of altimeter-derived gravity, the research area is divided into four regions, namely regions A, B, C, and D. As shown in Fig. 11, there are Dongsha, Xisha, and Zhongsha islands in region A. Regions B, C, and D include Nansha Islands, Philippine Islands, and Taiwan Island, respectively. NCEI shipborne data are distributed evenly in the SCS, and altimetric gravity anomalies in different regions are compared with NCEI data, as listed in Table 9. GSRL has higher precision than GC2 in the four regions, particularly in regions B and C, which include many islands and reefs. The results indicate that the precision of gravity derived from Ka-band altimeter data is superior to that derived from Ka-band altimeter data in the SCS, especially in areas with many islands and reefs.

Table 10
Statistics of differences between satellite-derived gravity and SIO V27.1 (mGal)

Distance from coastline	Data	Max.	Min.	Mean	STD	RMS
≥ 0	GSRL-V27.1	90.26	-92.99	-0.02	4.39	4.39
	GC2-V27.1	83.68	-92.30	-0.02	4.66	4.66
≤ 30 km	GSRL-V27.1	90.26	-92.99	0.19	8.67	8.67
	GC2-V27.1	83.68	-92.30	0.18	9.07	9.07

Finally, GSRL and GC2 are compared with marine gravity model SIO V27.1, and the results are presented in Table 10. It can be concluded that the precision of GSRL is higher than that of GC2. Compared with SIO V27.1, the difference STD for GSRL is 0.4 mGal and 0.27 mGal less than that for GC2 in the area within 30 km from the coastline and in the SCS, respectively. The results further indicate that the precision of Ka-band altimeter-derived gravity is higher compared with that of Ku-band altimeter-derived gravity, particularly in offshore areas.

7. Conclusions

SRL is the first altimetry satellite with a Ka-band radar altimeter. The purpose of this study is to evaluate the advantages of the Ka-band altimeter over Ku-band altimeters for SSH observation and marine gravity derivation. First, waveform data of SRL, Jason-2, and CryoSat-2 are used to study the radius of coastal influence on waveforms. Second, advantages of SRL/ERM in SSH observation over Jason-2/ERM are validated by crossover discrepancies, comparison with MSS models, and comparison with TG records, respectively. Finally, gridded gravity models GSRL and GC2 are derived from SSHs of SRL/DP and CryoSat-2, respectively. Shipborne gravity and SIO V27.1 are used to assess the precision of the two models. The following results are obtained:

Some ground tracks of SRL/ERM have large drifting from nominal tracks. The maximum drifting is approximately 10 km in the SCS, much larger than the designed ground track control band of ± 1 km. The radius of coastal influence on SRL/ERM is the smallest, being about 3 km. The STDs of crossover

discrepancies of SRL/ERM are about 3 mm and 12 mm less than those of Jason-2/ERM in the SCS and offshore areas, respectively. Compared with DTU18MSS, the difference STD for Jason-2/ERM is 7 mm and 23 mm greater than those for SRL/ERM in the SCS and offshore areas, respectively. Moreover, the correlation between TG data and SRL/ERM-measured SSHs is slightly stronger than that between TG data and Jason-2/ERM-measured SSHs. Assessed by NCEI, the precision of GSRL is 0.12 mGal higher than that of GC2 in the SCS, and 0.25 mGal higher in offshore areas. The difference STDs between GSRL and SIO V27.1 are 0.27 mGal and 0.4 mGal less than those when replacing GSRL with GC2 in the SCS and offshore areas, respectively.

Conclusions are drawn as follows: Compared with the traditional Ku-band altimeter, the Ka-band altimeter carried on SRL has a smaller footprint and higher frequency. Moreover, the coastline has a smaller contamination radius in the Ka-band waveform data. The SSH precision and altimeter-derived gravity precision of the Ka-band altimeter are higher than those of Ku-band altimeters in the SCS, especially in offshore areas. Due to the above advantages of the Ka-band altimeter carried on SRL, it is necessary to increase the weight of SRL observations when global MSS and marine gravity models are established from multisatellite altimeter data.

8. Availability of Data and Material

The datasets generated during and/or analyzed during the current study are available from the corresponding author on reasonable request, except for shipborne gravity data from MNR.

Acknowledgements

We are very grateful to AVISO and ESA for providing altimeter data. We are very grateful to NCEI and Second Institute of Oceanography of MNR, China, for providing shipborne gravimetric data. This study is supported by the National Natural Science Foundation of China (Grant Nos. 41774001, 41374009), the SDUST Research Fund (Grant No. 2014TDJH101), and Fujian Natural Science Foundation (Grant No. 2019J01649).

Authors' contributions X.L. and J.G. designed the research. C.Z., S.Y., and J.Y. developed the algorithm. C.Z., Y.N., Z.L., and Y.G. analyzed data. C.Z. wrote the manuscript with contributions from X.L., J.G., and J.Y. All authors were involved in discussions throughout the development.

Funding

This study is supported by the National Natural Science Foundation of China (grant nos. 41774001, 41374009), the SDUST Research Fund (grant no. 2014TDJH101), and Fujian Natural Science Foundation (grant no. 2019J01649).

Code availability

The code used during the current study is available from the corresponding author on reasonable request.

Declarations

Conflict of interest No conflicts of interest exist in the submission of this manuscript.

Publisher's Note Springer Nature remains neutral with regard to jurisdictional claims in published maps and institutional affiliations.

REFERENCES

- Andersen, O. B., Jain, M., & Knudsen, P. (2015). The impact of using Jason-1 and Cryosat-2 geodetic mission altimetry for gravity field modeling. In C. Rizos & P. Willis (Eds.), *IAG 150 Years*. (pp. 205–210). Springer. https://doi.org/10.1007/1345_2015_95.
- Andersen, O. B., Knudsen, P., & Stenseng, L. (2015). The DTU13 MSS (mean sea surface) and MDT (mean dynamic topography) from 20 years of satellite altimetry. In S. Jin & R. Barzaghi (Eds.), *IGFS 2014*. (pp. 111–121). Springer. https://doi.org/10.1007/1345_2015_182.
- Andersen, O. B., Knudsen, P., & Stenseng, L. (2018). A new DTU18 MSS mean sea surface—improvement from SAR altimetry. *25 Years of Progress in Radar Altimetry Symposium*. Abstracts, 172.
- Babu, K. N. (2014). Absolute calibration of SARAL-Altika in Kavaratti during its initial calibration validation phase. SARAL International Science and Applications Meeting. <http://www.aviso.altimetry.fr/fileadmin/documents/ScienceTeams/Saral2014/22-04-2014/Session-3/KNBabuAltikaApril2014.pdf>
- Brown, G. S. (1977). The average impulse response of a rough surface and its applications. *IEEE Journal of Ocean Engineering*, 2(1), 67–74.
- Caldwell, P. C., Merrifield, M. A., & Thompson, P. R. (2015). Sea level measured by tide gauges from global oceans—the Joint Archive for Sea Level Holdings (NCEI Accession 0019568), Version 5.5. *NOAA National Centers for Environmental Information, Dataset*, 10: V5V40S7W
- Cartwright, D. E., & Edden, A. C. (1973). Corrected tables of tidal harmonics. *Geophysical Journal Royal Astronomical Society*, 33(3), 253–264. <https://doi.org/10.1111/j.1365-246x.1973.tb03420.x>.
- CNES (2016). SARAL/Altika products handbook. SALP-MU-M-OP-15984-CN, Issue 2.5.
- CNES (2017). Along-track level-2+ (L2P) SLA product handbook. SALP-MU-P-EA-23150-CLS, Issue 1.0. https://www.aviso.altimetry.fr/fileadmin/documents/tools/hdbk_L2P_all_missions_except_S3.pdf
- Desai, S., Wahr, J., & Beckley, B. (2015). Revisiting the pole tide for and from satellite altimetry. *Journal of Geodesy*, 89(12), 1233–1243. <https://doi.org/10.1007/s00190-015-0848-7>.
- Guo, J., Chang, X., Hwang, C., Sun, J., & Han, Y. (2010). Oceanic surface geostrophic velocities determined with satellite altimetric crossover method. *Chinese Journal of Geophysics*, 53(6), 926–936. <https://doi.org/10.3969/j.issn.0001-5733.2010.11.006> in Chinese.
- Guo, J., Wang, J., Hu, Z., Hwang, C., Chen, C., & Gao, Y. (2015). Temporal-spatial variations of sea level over Chinese seas derived from altimeter data of TOPEX/Poseidon, Jason-1 and Jason-2 from 1993 to 2012. *Chinese Journal of Geophysics*, 58(9), 3103–3120. <https://doi.org/10.6038/cjg20150908> in Chinese.
- Hernandez, F., & Schaeffer, P. (2001). *The CLS01 mean sea surface: a validation with the GSF00.1 Surface*. . CLS Ramonville.
- Hsiao, Y., Hwang, C., Cheng, Y., Chen, L., Hsu, H., Tsai, J., Liu, C., Wang, C., & Kao, Y. (2016). High-resolution depth and coastline over major atolls of South China Sea from satellite altimetry and imagery. *Remote Sensing of Environment*, 176, 69–83. <https://doi.org/10.1016/j.rse.2016.01.016>.
- Hwang, C. (1998). Inverse Vening Meinesz formula and deflection-geoid formula: applications to the predictions of gravity and geoid over the South China Sea. *Journal of Geodesy*, 72(5), 304–312. <https://doi.org/10.1007/s001900050169>.
- Hwang, C., & Chang, E. (2014). Seafloor secrets revealed. *Science*, 346, 32–33. <https://doi.org/10.1126/science.1260459>.

- Hwang, C., & Parsons, B. (1995). Gravity anomalies derived from Seasat, Geosat, ERS-1 and TOPEX/POSEIDON altimetry and ship gravity: a case study over the Reykjanes Ridge. *Geophysical Journal International*, 122(2), 551–568. <https://doi.org/10.1111/j.1365-246X.1995.tb07013.x>.
- Hwang, C., Hsu, H., & Jang, R. (2002). Global mean sea surface and marine gravity anomaly from multi-satellite altimetry: applications of deflection-geoid and inverse Vening Meinesz formulae. *Journal of Geodesy*, 76(8), 407–418. <https://doi.org/10.1007/s00190-002-0265-6>.
- Kosempa, M., & Chambers, D. P. (2014). Southern Ocean velocity and geostrophic transport fields estimated by combining Jason altimetry and Argo data. *Journal of Geophysical Research: Oceans*, 119(8), 4761–4776. <https://doi.org/10.1002/2014jc009853>.
- Lickley, M. J., Hay, C. C., Tamisiea, M. E., & Mitrovica, J. X. (2018). Bias in estimates of global mean sea level change inferred from satellite altimetry. *Journal of Climate*, 31(13), 5263–5271. <https://doi.org/10.1175/jcli-d-18-0024.1>.
- Morton, B., & Blackmore, G. (2001). South China Sea. *Marine Pollution Bulletin*, 42(12), 1236–1263. [https://doi.org/10.1016/S0025-326X\(01\)00240-5](https://doi.org/10.1016/S0025-326X(01)00240-5).
- Pavlis, N. K., Holmes, S. A., Kenyon, S. C., & Factor, J. K. (2012). The development and evaluation of the Earth Gravitational Model 2008 (EGM2008). *Journal of Geophysical Research*, 117(B4), B04406. <https://doi.org/10.1029/2011jb008916>.
- Prandi, P., Philipps, S., Pignot, V., & Picot, N. (2015). SARAL/AltiKa global statistical assessment and cross-calibration with Jason-2. *Marine Geodesy*, 38(sp1), 297–312. <https://doi.org/10.1080/01490419.2014.995840>.
- Pujol, M., Schaeffer, P., Faugère, Y., Raynal, M., Dibarboure, G., & Picot, N. (2018). Gauging the improvement of recent mean sea surface models: a new approach for identifying and quantifying their errors. *Journal of Geophysical Research: Oceans*, 123(8), 5889–5911. <https://doi.org/10.1029/2017jc013503>.
- Rio, M., Mulet, S., & Picot, N. (2014). Beyond GOCE for the ocean circulation estimate: synergetic use of altimetry, gravimetry, and in situ data provides new insight into geostrophic and Ekman currents. *Geophysical Research Letters*, 41(24), 8918–8925. <https://doi.org/10.1002/2014gl061773>.
- Sandwell, D. T., Garcia, E., Soofi, K., Wessel, P., Chandler, M., & Smith, W. H. F. (2013). Toward 1-mGal accuracy in global marine gravity from CryoSat-2, Envisat, and Jason-1. *Leading Edge*, 32(8), 892–899.
- Sandwell, D. T., Muller, R. D., Smith, W. H. F., Garcia, E., & Francis, R. (2014). New global marine gravity model from CryoSat-2 and Jason-1 reveals buried tectonic structure. *Science*, 346, 65–67. <https://doi.org/10.1126/science.1258213>.
- Sandwell, D. T., Harper, H., Tozer, B., & Smith, W. H. F. (2019). Gravity field recovery from geodetic altimeter missions. *Advances in Space Research*. <https://doi.org/10.1016/j.asr.2019.09.011>.
- SARAL. (2015). Saral GDR quality assessment report cycle 024 28–05–2015/02–07–2015. SALP-RP-P2-EA-22250-CLS024, Issue 01.1.
- Schaeffer, P., Faugere, Y., Legeais, J. F., Ollivier, A., Guinle, T., & Picot, N. (2012). The CNES CLS11 global mean sea surface computed from 16 years of satellite altimeter data. *Marine Geodesy*, 35(sp1), 3–19. <https://doi.org/10.1080/01490419.2012.718231>.
- Shih, H., Hwang, C., Barriot, J. P., Mouyen, M., Corrêa, P., Lequeux, D., & Sichoix, L. (2015). High-resolution gravity and geoid models in Tahiti obtained from new airborne and land gravity observations: data fusion by spectral combination. *Earth, Planets and Space*, 67(1), 124. <https://doi.org/10.1186/s40623-015-0297-9>.
- Smith, W. H. F. (2015). Resolution of seamount geoid anomalies achieved by the SARAL/AltiKa and Envisat RA2 satellite radar altimeters. *Marine Geodesy*, 38(sp1), 644–671. <https://doi.org/10.1080/01490419.2015.1014950>.
- Yuan, J., Guo, J., Liu, X., Zhu, C., Niu, Y., Li, Z., Ji, B., & Ouyang, Y. (2020). Mean sea surface model over China seas and its adjacent ocean established with the 19-year moving average method from multi-satellite altimeter data. *Continental Shelf Research*, 192(1), 104009. <https://doi.org/10.1016/j.csr.2019.104009>.
- Zhang, S., & Sandwell, D. T. (2016). Retracking of SARAL/AltiKa radar altimetry waveforms for optimal gravity field recovery. *Marine Geodesy*, 40(1), 40–56.
- Zhu, C., Guo, J., Hwang, C., Gao, J., Yuan, J., & Liu, X. (2019). How HY-2A/GM altimeter performs in marine gravity derivation: assessment in the South China Sea. *Geophysical Journal International*, 219(2), 1056–1064. <https://doi.org/10.1093/gji/ggz330>.
- Zhu, C., Guo, J., Gao, J., Liu, X., Hwang, C., Yu, S., Yuan, J., Ji, B., & Bin, G. (2020). Marine gravity determined from multi-satellite GM/ERM altimeter data over the South China Sea: SCSGA V1.0. *Journal of Geodesy*, 94, 50. <https://doi.org/10.1007/s00190-020-01378-4>.